Received: Added at production | Revised: Added at production | Accepted: Added at production

DOI: xxx/xxxx

RESEARCH ARTICLE

Heat flow inside a catalyst particle for steam methane reforming: CFD-modeling and analytical solution

Dmitry Pashchenko[1] | Anton Eremin[1]

[1]Samara State Technical University, Molodogvardeiskaya str. 244, Samara, 443100, Russia

Correspondence
*Dmitry Pashchenko. Email: pashchenkodmitry@mail.ru

Present Address
Samara State Technical University, Molodogvardeiskaya str. 244, Samara, 443100, Russia

Summary

Numerical investigation of a steam methane reforming process was performed from point of view to understand the heat flows inside a catalyst particle. To verify the numerical results, a new method based on the thermal conductivity equation has been developed to determine the temperature distribution inside the catalyst particle. The CFD-model was realized via ANSYS Fluent. To model the steam methane reforming process, the industrial Ni-based catalyst with a spherical particle was chosen. The temperature contours inside the catalyst particle and hydrogen mole fraction in the reaction space was calculated both numerically and analytically. The results show the irregularity in the distribution of the temperature field inside the catalyst. In the direction of flow, a minimum catalyst temperature occurs. In this case, the temperature decrease inside the catalyst occurs unevenly. Also, the temperature change on the catalyst surface as a function of flow time was analyzed.

KEYWORDS:
CFD-modeling, steam methane reforming, thermal conductivity, temperature distribution

1 | INTRODUCTION

Computational fluid dynamics modeling (CFD-modeling) of various physical and chemical processes has recently been widely used by engineers and scientists in many countries. Various special software is used for CFD-modeling, among which such programs as ANSYS [1,2], Comsol [3], Autodesk Simulation CFD [4], OpenFOAM (open source) are most widely used. Some researchers are developing their own code to solve the problem of numerical simulation of steam methane reforming process [5]. Also, the constant increase in the computing power of personal computers makes it possible to use CFD-modeling for a wide range of researchers.

Among the problems that can be solved using CFD-modeling, an important place is occupied by CFD-modeling of the methane steam reforming (SMR) process[6,7,8]. In recent years, notable successes have been achieved in the numerical study of the SMR process. There are a large number of publications that discuss various aspects of the numerical simulation of SMR: the effect of technological parameters, the effect of geometric dimensionality of the computational domain, local transport and reaction rates, etc. The importance of CFD modeling of SMR is determined primarily by the wide application of this process in the industry: chemistry, energy, transport, etc. Tran et. al presented the results of CFD modeling of the SMR process in the industrial-scale steam methane reforming furnaces[9]. The authors concluded that a CFD-model of the steam methane reformer can be considered to be an adequate representation of the on-line reformer and can be used to determine the risk to operate the on-line reformer at un-explored and potentially more beneficial operating conditions. In addition, Lao et al. published the results of numerical investigation and control of the industrial steam methane reforming reactor via CFD-modeling[10]. They numerically investigated the industrial-scale top-fired co-current reformer that heated by natural gas combustion.

Most of the works dealing with CFD-modeling of SMR investigate the distribution of temperature, velocity, species concentration, etc. in the reaction zone. The results of these simulations can be verified using experimental data, which can be obtained using relatively simple laboratory facilities. Despite the notable successes achieved in the CFD-modeling of methane steam reforming, there are still a large number of practically interesting problems that need to be solved. One of these tasks is to study the temperature distribution inside a catalyst particle when SMR occurs. The complexity of this task lies in the fact that the experimental results inside the catalyst particles are rather difficult to obtain. However, experimental data are an important component for verifying the CFD-modeling results.

In this study, CFD-modeling of the steam methane reforming process over a pre-heated Ni-based catalyst was performed to determine the temperature distribution inside the catalyst. Moreover, to verify the CFD-modeling results, a new method has been developed to determine the temperature distribution inside the catalyst particle, based on the thermal conductivity equation. The objectives of the study are:

- CFD modeling of the SMR processes and determination of temperature distribution in the catalyst;
- Development of a new method for the analytical determination of the temperature distribution in the catalyst.

2 | CFD-MODELING

2.1 | Computational domain and mesh

Typically, the steam methane reforming process is carried out in the reformers with a fixed bed, which is filled with the catalyst particles. The shapes of the catalyst are different: cylinders, spheres, Raschig rings, etc. The effect of the catalyst shapes certainly

affects the reforming characteristics[11]. The main advantage of CFD-modeling is the fact that catalysts of various shapes can be used for modeling.

In this study, the computational domain is selected taking into account the further prospects of verification using numerical methods. Therefore, the cylindrical catalyst is selected for the computational domain. In addition, several assumptions and simplifications were made in the computational domain: the reaction space contains one catalyst particle 40 mm in diameter; the reformer wall is adiabatic; the catalyst temperature and the temperature of the initial reaction mixture are the same at the initial time.

A flow region with no reaction is added before the catalyst particle to obtain a developed flow near a catalyst particle. The schematic view of the computational domain is presented in Fig.1.

The steam methane reforming process mainly consists of three reversible reactions[12]: the endothermic reforming reactions (1) and (3), and the slightly exothermic water-gas shift reaction (2):

$$CH_4 + H_2O = CO + 3H_2, -\Delta H_{298} = -206.1 kJ/mol; \tag{1}$$

$$CO + H_2O = CO_2 + H_2, -\Delta H_{298} = +41.15 kJ/mol; \tag{2}$$

$$CH_4 + 2H_2O = CO_2 + 4H_2, -\Delta H_{298} = -165.0 kJ/mol. \tag{3}$$

In the computational domain, chemical reactions occur on the catalyst. Heat for the reaction is supplied by reaction flow. The input heat is consumed during endothermic reactions of the SMR process. There is no heat flow through the wall. Such a process corresponds to methane reforming over a pre-heated catalyst[?].

The length of the reaction space is 200 mm, the diameter is 80 mm. The physical property catalyst is shown in Table 1.

The mesh for the computational domain in Fig.1 contains about 2 million elements. The number of mesh elements and their structure is determined by the mesh independence study. To get a more perfect grid, the inflation layers around the catalyst were added in the fluid domain. Moreover, the inflation layer is also added near the tube wall in the fluid domain. The total thickness of the inflation layer is adjusted to get $20 < y^+ < 250$, a requirement for k-ϵ turbulence model.

2.2 | Governing equations

The CFD-model of the steam methane reforming process was realized via ANSYS Fluent on Xeon E5-2670 Sandy Bridge-EP server with double 20-core processors. In the model, the conservation equation of mass, momentum and energy equation in combination with species transport equations were solved in ANSYS Fluent 18.2. The transient flow was modeled. Moreover, the

following assumptions are taken for the model: no the flux of energy due to a mass concentration gradient (no Duflor effects)[?] ; work by viscous forces and by pressure is not done; surface oxidation reactions of the metal wall are absent.

The equation for conservation of mass, or continuity equation, for transient conditions, can be written as follows:

$$\frac{\partial \rho}{\partial t} + \boldsymbol{\nabla} \cdot (\rho \vec{v}) = 0 \tag{4}$$

The momentum equation in an inertial (non-accelerating) reference frame is described by follow equations[?] :

$$\frac{\partial}{\partial t}(\rho \vec{v}) + \nabla \cdot (\rho \vec{v} \vec{v}) = -\nabla \cdot p + \nabla \cdot (\bar{\bar{\tau}}) + \rho \vec{g} + \vec{F} \tag{5}$$

where p is the static pressure; $\rho \vec{g}$ and $\vec{F}$ are the gravitational body force and external body forces, respectively. The stress tensor $\bar{\bar{\tau}}$ is given by follows equation:

$$\bar{\bar{\tau}} = \mu \left[(\nabla \vec{v} + \vec{v}^{\mathrm{T}}) - \frac{2}{3} \nabla \cdot \vec{v} I \right] \tag{6}$$

where μ is the molecular viscosity, I is the unit tensor, and the second term on the right hand side is the effect of volume dilation.

The energy conservation equation for each reaction space in the reaction zone can be written as follows:

$$\nabla \cdot \vec{u}(p + \rho \cdot h_f) = \nabla \cdot \left[k_{eff} \cdot \nabla T - \left(\sum h_j \cdot \vec{J}_j \right) + \bar{\bar{\tau}} \cdot \vec{v} \right] + S_f^h \tag{7}$$

In this equation T is the reaction mixture temperature; ρ is the density; h_f is enthalpy of gas mixture; $\vec{J}_j$ is the diffusion flux of j element; k_{eff} is the conductivity; h_j is the enthalpy of j element; S_f^h is the fluid enthalpy source term (include the source of energy due to chemical reaction).

The energy conservation equation for the reformer walls can be written as follows:

$$\nabla \cdot (k_w \cdot \nabla T) = 0 \tag{8}$$

where k_w is the thermal conductivity of a wall.

Transport of j element of reaction mixture is described by follow equations:

$$\nabla \cdot (\rho \cdot \vec{v} \cdot Y_j) = -\nabla \vec{J}_j + R_j \tag{9}$$

where R_j is chemical reaction rate of species j formation or decomposition; Y_j is the mass fraction of j element of reaction mixture; $\vec{J}_j$ is diffusion flux of j species.

Diffusion flux of j species can be written as:

$$\vec{J}_j = -\left(\rho \cdot D_{j,m} + \frac{\mu_t}{Sc_t} \nabla Y_j - D_{T,j} \frac{\nabla T}{T} \right) \tag{10}$$

where $D_{j,m}$ and $D_{T,j}$ are the mass diffusion coefficient and thermal diffusion coefficient for j species, respectively; Sc_t and μ_t are the turbulent Schmidt number and turbulent viscosity, respectively.

2.3 | Turbulence model

Typically, the steam methane reforming is carried out as the laminar flow of the reaction mixture. The flow around the catalyst particle may have a vortex after particle; thereby using a laminar model may give an error in the results. The choice of turbulence model depends on considerations such as the physics encompassed in the flow, the established practice for a specific class of problem, the level of accuracy required, the available computational resources, and the amount of time available for the simulation. For present numerical model, the RNG k-ϵ model is chosen[??].

$$\frac{\partial}{\partial x_i}(\rho k v_i) = \frac{\partial}{\partial x_j}\left(\alpha_k \mu_{eff}\frac{\partial k}{\partial x_j}\right) + G_k + G_b - \rho\epsilon - Y_M + S_k \tag{11}$$

and

$$\frac{\partial}{\partial x_i}(\rho \epsilon v_i) = \frac{\partial}{\partial x_j}\left(\alpha_\epsilon \mu_{eff}\frac{\partial \epsilon}{\partial x_j}\right) + C_{1\epsilon}\frac{\epsilon}{k}(G_k + C_{3\epsilon}G_b) - C_{2\epsilon}\rho\frac{\epsilon^2}{k} - R_\epsilon + S_\epsilon \tag{12}$$

In equations for k-ϵ turbulence model, G_k shows the generation of turbulence kinetic energy due to the mean velocity gradients. G_b is the generation of turbulence kinetic energy due to buoyancy. Y_M represents the contribution of the fluctuating dilatation in compressible turbulence to the overall dissipation rate. The quantities α_k and α_ϵ are the inverse effective Prandtl numbers for k and ϵ, respectively. S_k and S_ϵ are user-defined source terms.

The additional term R_ϵ in the ϵ equation can be determined as follows:

$$R_\epsilon = \frac{C_\mu \rho \eta^3 (1 - \eta/\eta_0)}{1 + \beta\eta^3}\frac{\epsilon^2}{k} \tag{13}$$

where $\eta \equiv Sk/\epsilon$, $\eta_0 = 4.38$, $\beta = 0.012$.

The model constants $C_{1\epsilon}$ and $C_{2\epsilon}$ in k-ϵ turbulence model used by default setup for Fluent solver of ANSYS[?]:

$$C_{1\epsilon} = 1.42; \quad C_{2\epsilon} = 1.68 \tag{14}$$

2.4 | Kinetic model

The calculations of reaction rate for SMR process in present investigation are based on the nuanced analysis and investigations of chemical reactions that are presented in scientific publication[12,13]. It has been argued that both CH_4 and H_2O were adsorbed on the catalyst with dissociation. The expressions for determination of reaction rate suggested by Froment and Xu[12] are employed in this model.

The reaction rate of the methane consumption through reactions (1 and 3) can be found from following expression:

$$r_{CH_4} = R_1 + R_3. \tag{15}$$

The reaction rate of carbon monoxide (CO) and carbon dioxide (CO_2) production can be found from following expressions:

$$r_{CO} = R_1 - R_2. \tag{16}$$

$$r_{CO_2} = R_3 + R_2. \tag{17}$$

The rate of each reaction can be determined from following expressions[5]:

$$R_1 = \frac{k_1}{p_{H_2}^{2.5}} \left(p_{CH_4} \cdot p_{H_2O} - \frac{p_{H_2}^3 \cdot p_{CO}}{K_{e1}} \right) \cdot \frac{1}{Q_r^2}; \tag{18}$$

$$R_2 = \frac{k_2}{p_{H_2}} \left(p_{CO} \cdot p_{H_2O} - \frac{p_{H_2} \cdot p_{CO_2}}{K_{e2}} \right) \cdot \frac{1}{Q_r^2}; \tag{19}$$

$$R_3 = \frac{k_3}{p_{H_2}^{3.5}} \left(p_{CH_4} \cdot p_{H_2O}^2 - \frac{p_{H_2}^4 \cdot p_{CO_2}}{K_{e3}} \right) \cdot \frac{1}{Q_r^2}; \tag{20}$$

$$Q_r = 1 + K_{CO} \cdot p_{CO} + K_{H_2} \cdot p_{H_2} + K_{CH_4} \cdot p_{CH_4} + \frac{K_{H_2O} \cdot p_{H_2O}}{p_{H_2}}, \tag{21}$$

where p_i - partial pressure of i reacting element, bar; K_{je} - equilibrium constant of 1, 2, 3 reactions, respectively; k_j - kinetic rate constant of j reaction.

In eq.(21) adsorption constants of i element (K_i) can be determined as:

$$K_i = K_{0i} \cdot e^{-\Delta H_i/(R_0 T)}, \tag{22}$$

where H_i - adsorption enthalpy of i element, J/mol; K_{0i} - constant of i component.

2.5 | Boundary conditions

The specific heat and density of the reaction mixture are determined by the equations of mixing-law and incompressible-ideal-gas law, respectively. It can be possible because the temperature of the reaction mixture is moderate-high (less than 1000 K) and the pressure in the reaction space is moderate-low (less than 10 bar). Also, the Mach number is about 0.001 due to the low velocity of the reaction mixture. Therefore, the assumption for ideal incompressible gas flow is sufficiently provided. The viscosity of the gas flow is determined by Sutherland viscosity law. The thermal conductivity of the gas flow is computed as an average mass fraction of each element. The pressure-based solver is used. The convergence criterion for momentum, continuity, and species are defined as 10^{-3}, for energy less than 10^{-6}. The hybrid initialization is chosen to initialize calculation. For described equations, the Second-Order Upwind approximation method is used to obtain a higher calculation accuracy. When second-order

accuracy is desired, quantities at cell faces are computed using a multidimensional linear reconstruction approach[?] . The initial conditions for the model are presented in Table 2.

The boundary conditions for the computational domain of the reformer shown in Fig.1 are determined as follows:

- reformer inlet:

$$x = 0; T_g = T_{g(in)}; C_i = C_{i(in)}; T_g = T_{cat}. \tag{23}$$

- reformer outlet:

$$x = L; \frac{\partial C_i}{\partial x} = 0. \tag{24}$$

- reformer center:

$$y = 0; \frac{\partial C_i}{\partial y} = 0; \frac{\partial T_g}{\partial y} = 0. \tag{25}$$

where C_i is mole concentration of i element.

3 | RESULTS AND DISCUSSION

3.1 | Analytical solution

To verify the temperature and heat flux distribution model inside the catalyst particle, a new algorithm was developed. Such an algorithm allows us to obtain the exact distribution of temperature and heat flux inside the catalyst based on the fundamental equations of heat conduction.

The heat transfer process in the catalyst can be described by the parabolic heat equation. In the developed model, it is assumed that the thermophysical properties of the catalyst are isotropic and constant over time, therefore, the equation has the following form:

$$\frac{\partial T}{\partial t} = a\nabla^2 T + \frac{q_{smr}}{C_v}, \tag{26}$$

where T - temperature; t - time; $a = k/C_v$ - thermal diffusivity coefficient; k - thermal conductivity; $C_v = C_p \cdot \rho$ - specific volumetric heat capacity; ρ - density; q_{smr} - endothermic effect of the steam methane reforming process.

The last term of eq.(26) takes into account the absorption of heat due to the steam methane reforming reaction. To obtain a solution to equation (26), the boundary-value problem describing the temperature distribution in a spherical catalyst was considered. At the initial time, the temperature of the catalyst is equal to the temperature of the reaction mixture. On the surface of the catalyst, a boundary condition of the third kind is set with a constant temperature of the reaction mixture T_g and the heat transfer coefficient h. On the surface of the catalyst, there are uniformly distributed heat sinks caused by the endothermic reaction of the steam methane reforming process.

Given the isotropy of catalyst thermophysical properties, the uniform distribution of heat sinks and heat fluxes on the catalyst surface, as well as the constancy of the initial temperature at each point of the studied region, the temperature will be a function of two variables - spatial (r) and temporal (t). Therefore, eq.(26) cab be written as:

$$\frac{\partial T(r;t)}{\partial t} = a\left[\frac{2}{r}\frac{\partial T(r;t)}{\partial r} + \frac{\partial^2 T(r;t)}{\partial r^2}\right] + \frac{q_{smr}}{C_v}. \tag{27}$$

The boundary conditions for eq.(27) have the following form:

$$T(r;0) = T_0; \left.\frac{\partial T(r;t)}{\partial r}\right|_{r=0} = 0; -k\left.\frac{\partial T(r;t)}{\partial r}\right|_{r=R} = h(T(R;t) - T_g). \tag{28}$$

where h - heat-exchange coefficient; R - radius of the catalyst particle; T_g - reaction mixture temperature.

The solution of eq.(27) can be obtained by applying the Laplace integral transform. Using the transition tables to the originals of functions, the solution of eq.(27) has the following form:

$$T(r;t) = T_g + \frac{q_{smr}R^2}{6k}\left(1 + \frac{2kR}{h} - \frac{r^2}{R^2}\right) - \\ - \sum_{n=1}^{\infty}\left(T_g - T_0 + \frac{q_{smr}R^2}{k\mu_n^2}\right)A_n\frac{R\sin\left(\mu_n\frac{r}{R}\right)}{r\mu_n}exp\left(-\mu_n^2\frac{at}{R^2}\right). \tag{29}$$

The expression (29) is obtained for the case when the temperature of the catalyst is not equal to the temperature of the reaction mixture.

Using the approximate method[?] for solving equations (27)-(28), based on the introduction of a new function and additional boundary characteristics, a solution can also be found in the following form:

$$\Theta(\xi; Fo) = \frac{Po}{6}\left(\xi^2 - 1 - \frac{2}{Bi}\right)\exp(-\eta Fo) + \frac{Po}{6}\left(1 - \xi^2 + \frac{2}{Bi}\right) + 1. \tag{30}$$

where $\Theta(\xi; Fo) = \frac{T(r;t)}{T_0}$ - dimensionless temperature; $Po = \frac{q_{smr}R^2}{kT_0}$ - Pomerantsev criterion; $\eta = \frac{9Bi}{Bi+3}$; $Bi = \frac{h}{kR}$ - Biot number; ξ - relative coordinate; $Fo = \frac{a\cdot t}{R^2}$ - dimensionless time; $\xi = \frac{r}{R}$ - relative distance.

The enthalpy of the endothermic reaction was determined on the kinetic model suggested by Xu and Froment. The kinetic model was discussed above 2.4.

The equation (30) can be used in the case when the heat consumption is uniformly distributed over the entire body volume (according to the last term of equation (27)). If the source proceed only on the catalyst surface, boundary conditions for eq.(27) have the following form:

$$T(r;0) = T_0; \frac{\partial T(r;t)}{\partial r} = 0; -k\frac{\partial T(R;t)}{\partial r} = q_{smr} - h(T_g - T(R;t)). \tag{31}$$

The equation for determination of temperature distribution in the Catalyst particle will be written as follows:

$$\Theta(\xi; Fo) = \frac{B}{T_0}\left[\frac{3\exp(-\eta \cdot Fo)(T_0 B^{-1} - 1)Bi(1 + 2Bi^{-1} - \xi^2)}{2Bi + 3}\right] + 1 \tag{32}$$

where $B = T_g - \frac{q_{smr}}{h}$.

The equation (32) has great practical importance. Using a simple expression (32), it is possible to determine the temperature distribution in any catalyst whose thermal properties are known for any endothermic reaction. This suggests that the equation (32) can be used not only to model heat fluxes inside the catalyst for the steam reforming reaction but for other endothermic reactions.

3.2 | Contours and profiles

The results of CFD modeling are presented as the contours and profiles of various controlled parameters of the steam methane reforming process. The main advantage of the results of CFD modeling is the visibility of the results.

Fig.2 shows the temperature profiles inside the catalyst and the hydrogen mole fraction for a time on stream of 5 seconds. The initial data for the obtained results are as follows: the initial temperature of the catalyst is 1000K, the composition of the initial reaction mixture is H_2O:CH_4:H_2 = 2:1:0.15, and the flow rate of the reaction mixture is 1 m/s.

The results in Fig.2 are obtained when solving a non-stationary problem for a time moment of 5 seconds after the start of the flow. The CFD model was obtained via ANSYS Fluent 18.2 Academic version. Convergence for each numerical experiment took approximately 6000 iterations for which the computation time was on the order of 30 hours.

Fig.2 clearly shows the irregularity in the distribution of the temperature field inside the catalyst. In the direction of flow, a minimum catalyst temperature occurs. In this case, the temperature decrease inside the catalyst occurs unevenly. The maximum temperature of about 993 K does not occur in the center of the particle but is shifted in the direction opposite to the motion of the catalyst particles. Such an irregularity in the temperature change can be explained by the fact that in the frontal part of the catalyst the intensity of the methane steam reforming reaction is maximum. Moreover, in the back of the reaction intensity decreases.

In addition, Fig.2 shows the contours of the mole fraction of hydrogen. Fig.2 depicts that when passing the reaction mixture near the surface of the catalyst, the hydrogen concentration increases. This fact correlates well with the works of other authors.

To quantitatively compare the results of CFD modeling and numerical solutions, the temperature profile at various points in time was analyzed.

Fig.3 shows a temperature profile inside the catalyst. The solid line is the results of the analytical solution, the dashed line is the results of CFD modeling. In order to obtain the dependence of temperature on the radial position for CFD modeling, auxiliary circles were constructed. Therefore, in fig. Fig.3 shows the average temperature for each radial position within the catalyst.

Fig.3 shows that at the initial time, the temperature inside the catalyst is constant. Then, when the reaction mixture gets on the catalyst, the endothermic reaction of methane steam reforming begins to proceed. This reaction proceeds mainly on the surface of the catalyst; therefore, the temperature on the surface of the catalyst is lower than inside the catalyst. With an increase in the flow time, the temperature profile gradually becomes equal, and approximately 25 seconds after the start of the flow, the temperature inside the catalyst and on the surface becomes equal. With the help of such a study, an important conclusion can be made, namely, for the studied initial data, approximately 25 seconds after the start of the heat flux that contains the reaction mixture, it will be enough to compensate for the endothermic effect of the methane steam reforming reaction.

Fig.3 shows the temperature change on the catalyst surface as a function of flow time. Also, Fig.3 shows auxiliary circles for obtaining the results of CFD modeling. Fig.3 makes it clear that at a flow time of about 25 seconds, the temperature on the surface of the catalyst stabilizes.

4 | CONCLUSION

It has been shown that a commercial CFD code can be used to determine the heat flow inside a catalyst particle. To verify the results of CFD-modeling, the new method based on the thermal conductivity equation was developed. The new equation has great practical importance. Using a simple expression, it is possible to determine the temperature distribution in any catalyst whose thermal properties are known for any endothermic reaction. This suggests that the equation can be used not only to model heat fluxes inside the catalyst for the steam reforming reaction but for other endothermic reactions. The discrepancy between the results obtained via CFD-model and via new method was less 5%. Based on the CFD-model it was established the irregularity in the distribution of the temperature field inside the catalyst. In the direction of flow, a minimum catalyst temperature occurs. Also, the temperature change on the catalyst surface as a function of flow time was analyzed. It was established that at a time on stream of about 25 seconds, the temperature on the surface of the catalyst stabilizes.

ACKNOWLEDGMENT

This work is supported by the Russian Science Foundation under grant 19-19-00327.

References

1. Tran A, Aguirre A, Crose M, Durand H, Christofides PD. Temperature balancing in steam methane reforming furnace via an integrated CFD/data-based optimization approach. *Computers & Chemical Engineering* 2017; 104: 185–200.

2. Chen J, Yan L, Song W, Xu D. Methane steam reforming thermally coupled with catalytic combustion in catalytic microreactors for hydrogen production. *International Journal of Hydrogen Energy* 2017; 42(1): 664–680.

3. Corigliano O, Fragiacomo P. Numerical simulations for testing performances of an Indirect Internal CO 2 Reforming Solid Oxide Fuel Cell System fed by biogas. *Fuel* 2017; 196: 378–390.

4. Unseld M, Szepanski C, Lindermeir A, Maus-Friedrichs W, Dahle S. Desulfurization of Biogas via Dielectric Barrier Discharges. *Chemical Engineering & Technology* 2017; 40(2): 333–339.

5. Hoang D, Chan S, Ding O. Kinetic and modelling study of methane steam reforming over sulfide nickel catalyst on a gamma alumina support. *Chemical Engineering Journal* 2005; 112(1): 1–11.

6. Tran A, Aguirre A, Durand H, Crose M, Christofides PD. CFD Modeling of a Industrial-scale Steam Methane Reforming Furnace. *Chemical Engineering Science* 2017.

7. Nobandegani MS, Birjandi MRS, Darbandi T, Khalilipour MM, Shahraki F, Mohebbi-Kalhori D. An industrial Steam Methane Reformer optimization using response surface methodology. *Journal of Natural Gas Science and Engineering* 2016; 36: 540–549.

8. Diglio G, Hanak DP, Bareschino P, et al. Techno-economic analysis of sorption-enhanced steam methane reforming in a fixed bed reactor network integrated with fuel cell. *Journal of Power Sources* 2017; 364: 41–51.

9. Tran A, Pont M, Crose M, Christofides PD. Real-time furnace balancing of steam methane reforming furnaces. *Chemical Engineering Research and Design* 2018; 134: 238–256.

10. Lao L, Aguirre A, Tran A, Wu Z, Durand H, Christofides PD. CFD modeling and control of a steam methane reforming reactor. *Chemical Engineering Science* 2016; 148: 78–92.

11. Pashchenko D. Combined methane reforming with a mixture of methane combustion products and steam over a Ni-based catalyst: An experimental and thermodynamic study. *Energy* 2019; 185: 573–584.

12. Xu J, Froment GF. Methane steam reforming, methanation and water-gas shift: I. Intrinsic kinetics. *AIChE Journal* 1989; 35(1): 88–96.

13. Nguyen VN, Deja R, Peters R, Blum L. Methane/steam global reforming kinetics over the Ni/YSZ of planar pre-reformers for SOFC systems. *Chemical Engineering Journal* 2016; 292: 113–122.

14. Spallina V, Marinello B, Gallucci F, Romano MC, Annaland MVS. Chemical looping reforming in packed-bed reactors: modelling, experimental validation and large-scale reactor design. *Fuel Processing Technology* 2017; 156: 156–170.

15. Pan F, Cheng X, Wu X, Wang X, Gong J. Thermodynamic Design and Performance Calculation of the Thermochemical Reformers. *Energies* 2019; 12(19): 3693.

16. Elreedy A, Tawfik A, Enitan A, Kumari S, Bux F. Pathways of 3-biofules (hydrogen, ethanol and methane) production from petrochemical industry wastewater via anaerobic packed bed baffled reactor inoculated with mixed culture bacteria. *Energy conversion and management* 2016; 122: 119–130.

17. Inbamrung P, Sornchamni T, Prapainainar C, Tungkamani S, Narataruksa P, Jovanovic GN. Modeling of a square channel monolith reactor for methane steam reforming. *Energy* 2018; 152: 383–400.

TABLE 1 Catalyst properties.

Catalyst properties	Value
Nickel content (wt.%)	9.8
S content (wt.%)	4.9
Alumina content (wt.%)	85.3
Surface area (m^2/g)	155
Size of the sphere (mm)	40
Density (kg/m^3)	3960
Specific heat (J/kg·K)	880
Thermal conductivity (W/m·K)	33.15
Molecular Weight (kg/kgmol)	184.41

TABLE 2 Initial conditions

No.	Parameter	Inlet	Outlet
1	Steam-to-methane ratio	var	–
2	Temperature	var	–
3	Turbulent intensity	5 %	5 %
4	Hydraulic diameter	0.08 m	0.08 m
6	Gauge pressure	1.5 bar	0.0 bar

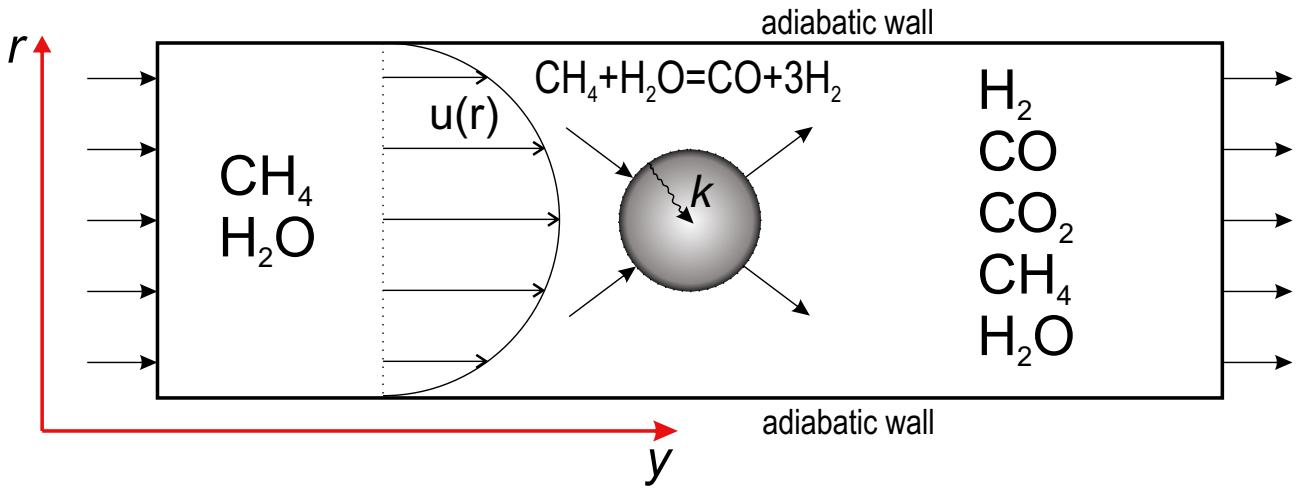

FIGURE 1 Computational domain for CFD-modeling and schematic diagram of the steam methane reforming process.

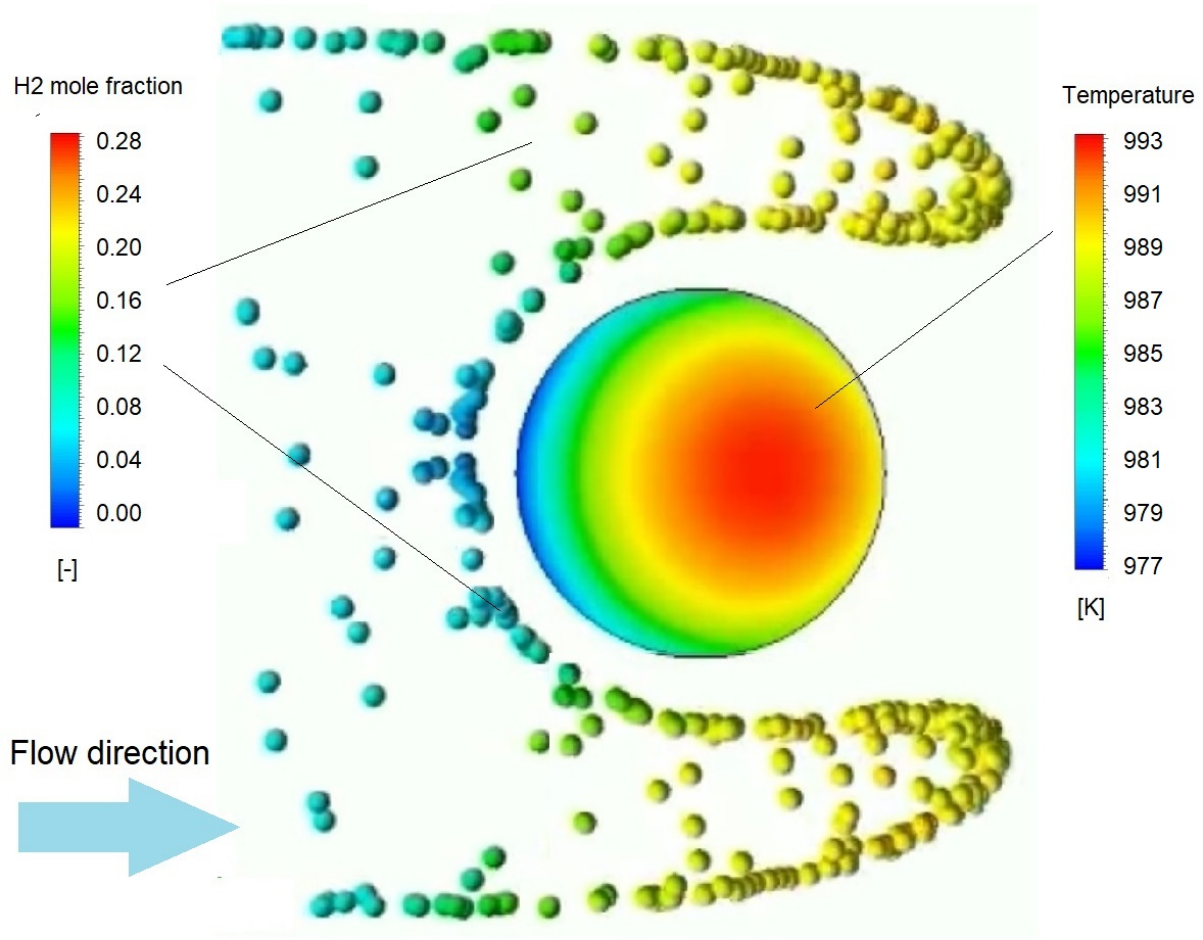

FIGURE 2 The temperature contour inside the catalyst particle and H_2 mole fraction in the reaction space.

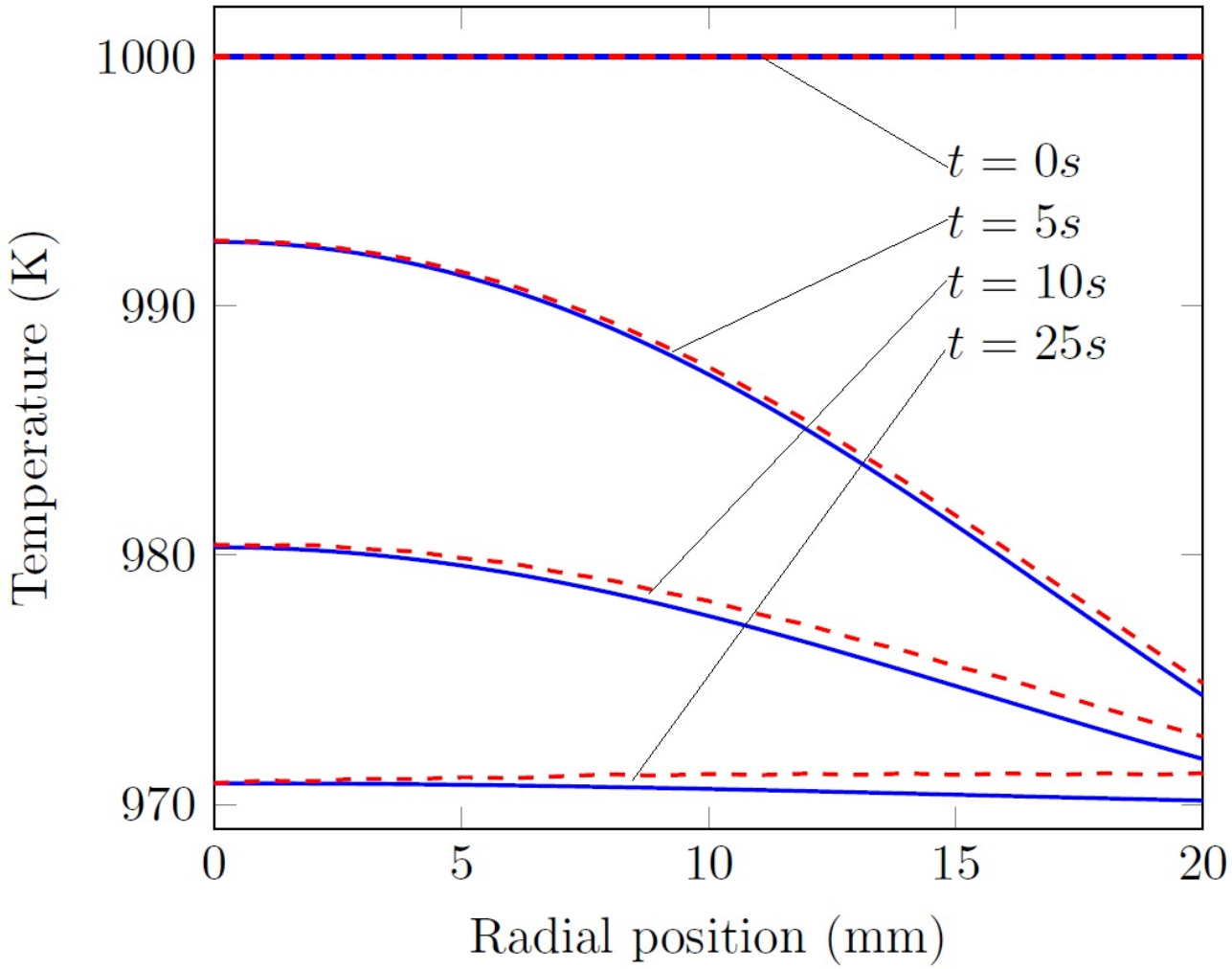

FIGURE 3 The temperature profiles inside the catalyst particle: solid line – analytical results; dashed line – results of CFD-modeling.

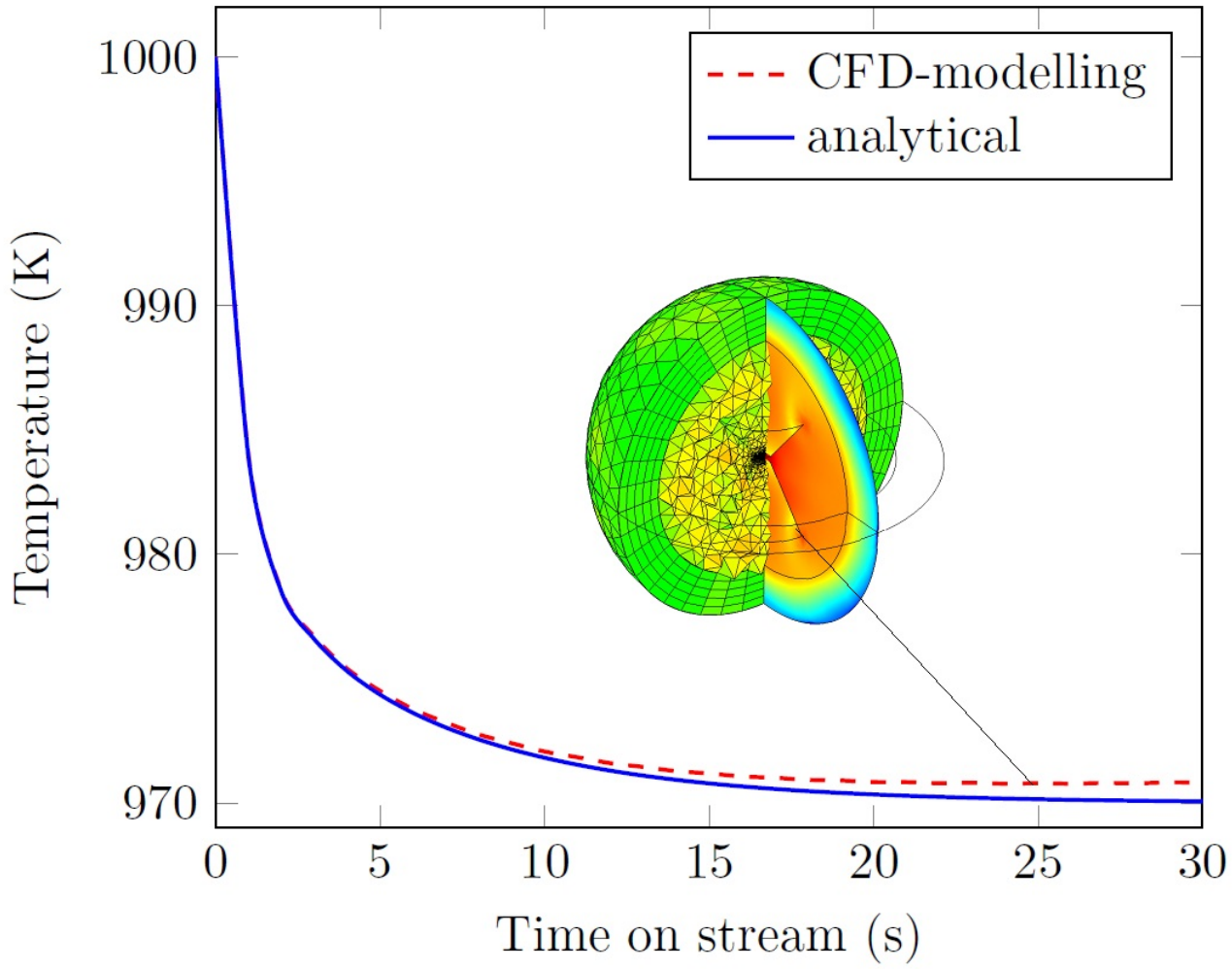

FIGURE 4 The temperature on the catalyst surface as a function of time on stream.